LANGMUIR

pubs.acs.org/Langmuir Article

Structural Diversity in Cryoaerogel Synthesis

Dennis Müller, Lars F. Klepzig, Anja Schlosser, Dirk Dorfs,* and Nadja C. Bigall

Cite This: *Langmuir* 2021, 37, 5109–5117 Read Online

ACCESS | Metrics & More | Article Recommendations | Supporting Information

ABSTRACT: Different techniques that enable the selective microstructure design of aerogels without the use of additives are presented. For this, aerogels were prepared from platinum nanoparticle solutions using the cryoaerogelation method, and respective impacts of different freezing times, freezing media, and freezing temperatures were investigated with electron microscopy as well as inductively coupled plasma optical emission spectroscopy. The use of lower freezing temperatures, freezing media with higher heat conductivities, and longer freezing periods led to extremely different network structures with enhanced stability. In detail, materials were created in the shape of lamellar, cellular, and dendritic networks. So far, without changing the building blocks, it was not possible to create the selective morphologies of resulting aerogels in cryoaerogelation. Now, these additive-free approaches enable targeted structuring and will open up new opportunities in the future cryoaerogel design.

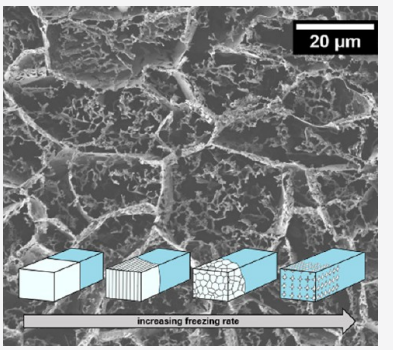

Downloaded via LEIBNIZ UNIVERSITAET HANNOVER on March 20, 2024 at 09:10:32 (UTC).
See https://pubs.acs.org/sharingguidelines for options on how to legitimately share published articles.

1. INTRODUCTION

Because of their unique physical properties such as high specific surface areas and open-pore structures, aerogels are highly investigated. Recently, those materials gained high interest in applications such as in catalyzed syntheses[1,2] as well as in electrocatalytic[3−5] and photocatalytic reactions.[6,7] Furthermore, a variety of sensing applications were reported.[8−10] Owing to the good accessibility of the surface, thin films or coatings from these materials experience an increasing interest.[11−13] In most cases, the aerogel coating is prepared by dropcasting and drying a slurry consisting of an aerogel material, solvents, and a binding substance like Nafion.[14−17] Because of mixing the slurry, however, the monolithic network is broken into smaller segments. In the resulting coating, these parts are later covered and connected using the binder. Thus, compared to pure and monolithic coatings, this procedure leads to a partial loss of the structure, hierarchical pore system, and accessible surface area.

A potential way to avoid this is offered by freeze-casting or ice-templating techniques, which can create monolithic and porous materials directly on the substrate. In general, freeze-casting processes use slurries from ceramic particles with additional additives such as polymeric binders and dispersants. This mixture is directionally frozen so that ice crystals nucleate and grow along the temperature gradient. Suspended ceramic particles are redistributed by segregation from the freezing front, and they assemble in the space between the crystals. After complete solidification, the templated ceramic is freeze-dried to sublime the ice template and leave a scaffold. Finally, this structure is sintered to consolidate particulate walls and provide stability to the porous material.[18−20]

A similar method for polymeric materials is the so-called cryogelation, which was implemented in the 1970s.[21] Following a controlled freeze/thaw cycle, in the cryogelation process, the temperature is decreased below the precursor solution freezing point. A large proportion of the solvent is crystallized, and monomers are concentrated in the liquid phase between the crystals. As time progresses, the gelation of monomers to the cross-linked polymer networks occurs. After thawing, spongelike, macroporous, and polymeric hydrogel structures are remaining, which are commonly called cryogels.[22,23] These types of materials are investigated for use in the fields of tissue engineering and a variety of biorelated applications.[24]

While freeze-casting and cryogelation techniques were limited to ceramic or polymeric materials, our workgroup recently developed a versatile strategy to create comparable structures from a variety of nanocrystal materials.[25] Because there is no chemical selectivity, both the ingredients as well as composition ratios are freely variable. This method results from a combination of ice-templating and gelation of colloidal nanoparticle solutions.

In the standard procedure of the so-called cryoaerogelation, a colloidal nanocrystal suspension is flash-frozen by means of liquid nitrogen. Because we inject or dip the sample directly into the freezing media, a basically nondirectional freezing process takes place. This ensures a uniform and sudden crystallization of the solvent within the colloidal solution. As a result, small ice crystallites are formed, which exclude the

Received: December 23, 2020
Revised: March 1, 2021
Published: April 22, 2021

ACS Publications

© 2021 The Authors. Published by American Chemical Society

https://doi.org/10.1021/acs.langmuir.0c03619
Langmuir 2021, 37, 5109−5117

nanoparticles during growth and push them into the space between. By that, an interconnected network of nanoparticles is established in the interstices of the ice template. Once solidified, the frozen ice template is removed by lyophilization in order to circumvent capillary forces. In contrast to other gelation methods, prior formation of a wet gel is skipped. A scheme of this procedure is displayed in Figure 1. So far,

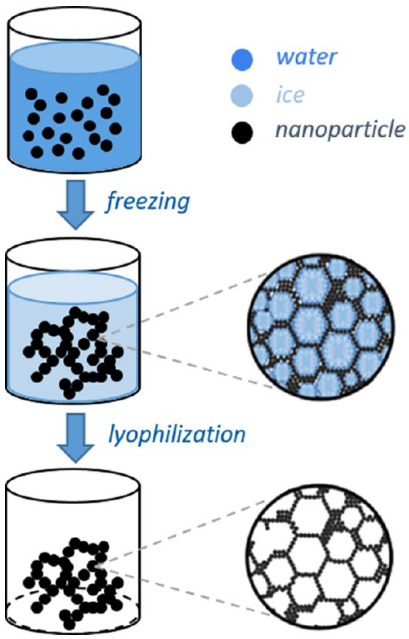

Figure 1. Schematic representation of cryoaerogelation procedures.

general requirements are that particles have to be in the aqueous solution and that their concentration must exceed a critical value (at least 0.1 vol %) in order to completely fill the network forming in the frozen state and hence provide sufficient mechanical stability upon ice removal. However, if this is the case, the shape of the resulting cryoaerogel resembles the shape of the frozen colloid.[25−27] Because of this fact, it is possible to create macroscopic shapes by the use of molds. Furthermore, we are able to produce thin films of resulting cryoaerogels by distributing the nanoparticle solution on substrates before freezing. It is to be noted that with this method, coatings are prepared without any binding additive, and the resulting films present a continuous network of nanoparticles that are in direct contact. In this way, the accessible surface is maximized compared to the conventional coatings from aerogels prepared by drop-casting a slurry of respective gels and a binding agent.

So far, successful applications of materials created using this technique has been shown by our workgroup in photoelectrochemical sensing with semiconductor-based cryoaerogel coatings.[28] Nevertheless, the poor stability of such aerogel coatings due to the destruction of their textural properties in wet applications is a well-known problem.[29]

Based on these problems and motivated by the high application potential of cryoaerogels, in the present work, we created cryoaerogel coatings from highly concentrated platinum nanoparticles (size: 3−5 nm) in an aqueous solution. For the first time, we varied the freezing speed by changing the freezing medium or setting different freezing temperatures and found significant impact on the resulting material network structure and their related stability. Especially, freezing media with boiling points above the substrate temperature (room temperature) show very different results than liquid nitrogen as the freezing medium from the standard technique. We also found an improvement in the quality of the resulting material when adjusting the duration of the freezing step before lyophilization. By changing each of these parameters, we reached a larger controlled structural diversity of the resulting cryoaerogels with improved stability when compared to the results from the previous standard procedure. This unexpected versatility for tuning highly porous and continuous coatings combined with the additive-free preparation technique offers promising approaches for the future aerogel design.

2. RESULTS AND DISCUSSION

2.1. Effect of Different Freezing Media. In the standard procedure of cryoaerogelation, the nanoparticle solution is applied and spread on the substrate. Afterward, the samples are flash-frozen by means of liquid nitrogen at its boiling point (77 K). Because the sample temperature (room temperature) is far above, nitrogen evaporates and forms a bubble wrap around the sample when getting into contact (Leidenfrost effect). The heat conductivity of this gaseous nitrogen shell is much lower than that of liquid nitrogen so that the bubble wrap effect leads to a decrease in the sample freezing speed. To avoid this delay in the freezing process and, on the contrary, increase the freezing speed, we replaced liquid nitrogen with different freezing media. To also avoid mixing with the aqueous solution, we chose nonpolar organic media, such as toluene, *n*-hexane, *n*-pentane, or isopentane and cooled them with liquid nitrogen to their respective melting points, which are stated in Table 1. Afterward, in each separate medium, the coatings of

Table 1. Temperatures of Freezing Media

nitrogen	*n*-hexane	toluene	*n*-pentane	isopentane
77 K	179 K	178 K	142 K	113 K

platinum nanoparticle solutions were flash-frozen and immediately freeze-dried. The resulting morphologies were investigated with scanning electron microscopy (SEM) and displayed in Figure 2.

The gel network structure differs significantly for different freezing media: in liquid nitrogen (Figure 2a-b), the bubble wrap of N_2 vapor seemingly leads to a lower freezing speed (despite the by far lowest temperature of all freezing media) and thus to a more noticeable directed freezing. Matching with the literature, this results in long-range ordered, lamellar ice templates.[30−32] The finally obtained aerogel network achieves an aligned and lamellar shape. However, when using freezing media like *n*-hexane or toluene that ensure higher heat conductivities (Figure 2c−f), the received aerogel networks are less aligned. The increase in the freezing speed leads to a faster nucleation of smaller ice crystals and more cell-like growth with random- or short-range ordered structures. These results are supported by Lottermoser,[33] who first discovered the growth of cellular templated ice.

Using freezing media, such as *n*-pentane and isopentane, at even lower temperatures causes an even faster nucleation of even smaller ice crystallites. Crystallization thus develops from cell growth to dendrite-like growth, which can be recognized in the finally obtained aerogel network (Figure 2g−j). On the one hand, nanoparticles are connected to already known sheet structures that now form cell-like networks. On the other hand,

https://doi.org/10.1021/acs.langmuir.0c03619
Langmuir 2021, 37, 5109−5117

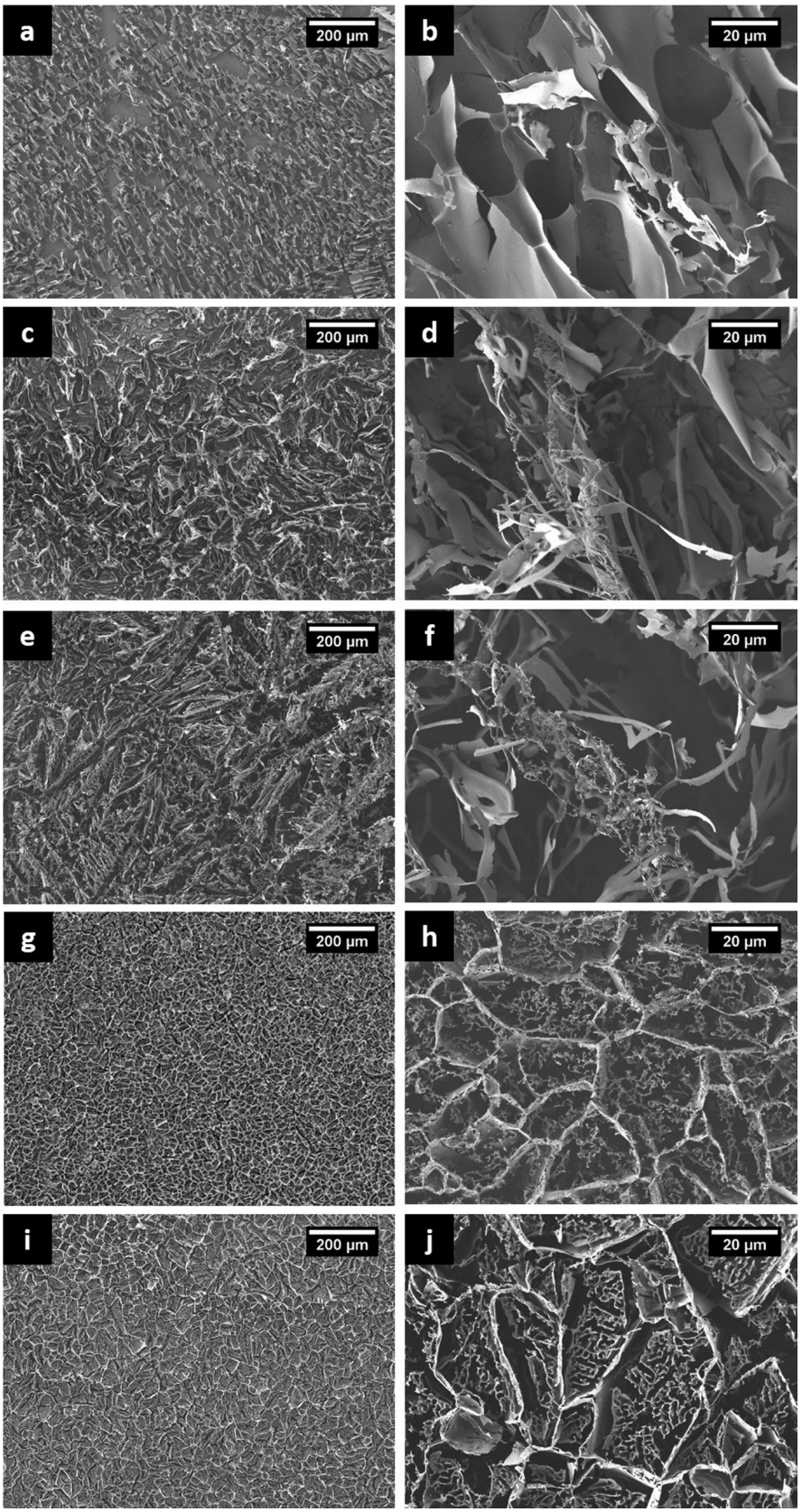

Figure 2. SEM images of platinum cryoaerogel coatings freeze-dried after flash-freezing in different media at their respective melting temperature: (a-b) liquid nitrogen (at 77 K), (c-d) *n*-hexane, (e-f) toluene, (g-h) *n*-pentane, and (i-j) isopentane.

the cells are further interconnected by dendrite-like gel networks. This can be supported by discoveries from Makkonen, who reported dendritic-grown ice as a result of uniform heat flux.[34]

https://doi.org/10.1021/acs.langmuir.0c03619
Langmuir 2021, 37, 5109−5117

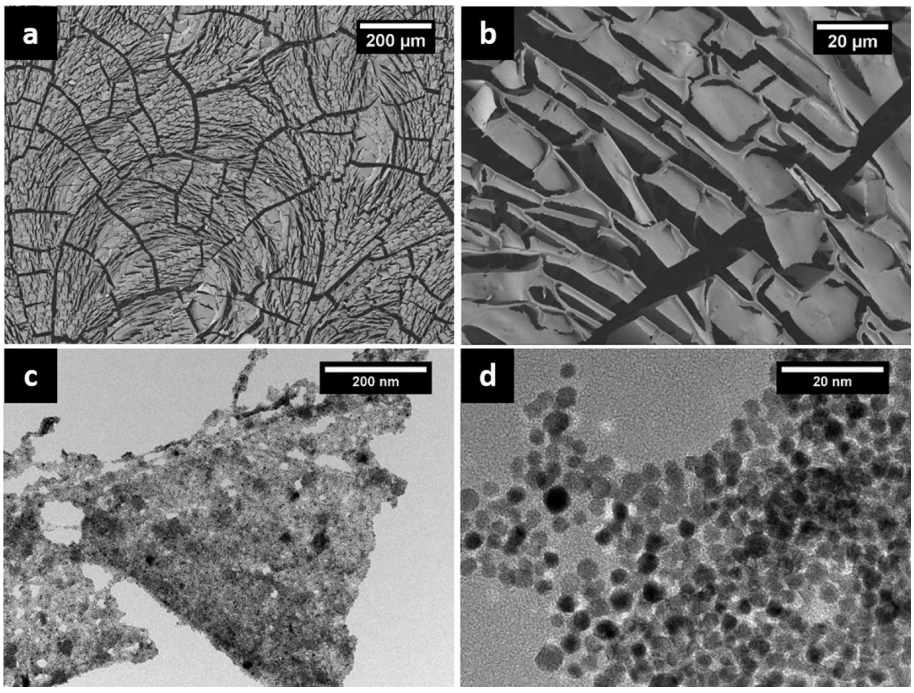

Figure 3. SEM (a-b) and TEM (c-d) images of a platinum nanoparticle coating freeze-dried after freezing inside a freezer at 253 K (in an air atmosphere).

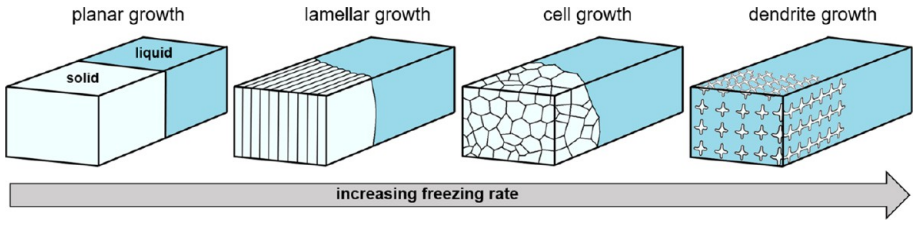

Figure 4. Influence of different freezing rates on the crystallization process of ice.

In contrast to the different network structures that can be seen in the SEM images (Figure 2), the nano- and crystal structures of the underlying aerogel segments and the nanoparticle building blocks seem to be the same in case of every freezing medium and consist of sheetlike structures of directly connected nanoparticles. In this context, Figure S3 presents the results from the transmission electron microscopy (TEM) measurements, and Figure S4 presents the results from the high-resolution TEM (HRTEM) measurements for the corresponding samples from Figure 2.

Freezing much faster would lead to amorphous ice (glassy water)[35] with completely entrapped but nongelated particles.[36] On the other hand, we performed very slow freezing in a cool air atmosphere at 253 K. Figure 3 displays the corresponding SEM and TEM images for the resulting coating material. With a slow freezing rate, only a few ice crystallites are formed, which grow to a bigger and planar ice front. Nanoparticles are excluded and pushed in front of the ice layer. Because of the (almost complete) absence of inner grain boundaries within the ice, the particles are expected to not experience the pressure pushing them closely together that occurs between growing ice crystallites (such as in the standard cryoaerogelation). In the end, this results in a uniform layer of poorly connected nanoparticles on top of the ice front. After freeze-drying, these materials can be distinguished by high fragility (because of the poor particle connection) and poor porosity, which is presumably a result of cracks during the drying process.

Figure 4 sums up the explained influence of the different freezing rates on the crystallization process and the formation of the resulting cryoaerogel network.

2.2. Influence of Freezing Temperatures. Apart from varying the medium, we also tuned the freezing speed by different cooling temperatures using the same freezing medium. In this regard, we prepared platinum cryoaerogel coatings by freezing in isopentane, which we cooled to 263, 223, 173, and 113 K. The resulting morphologies were investigated with SEM and are presented in Figure 5.

Decreasing the temperatures of the cooling medium lead to faster freezing of samples and a lower degree of orientation within the ice template.[37] As already discussed, slower freezing (at higher temperatures) results in aligned and lamellar shapes (Figure 5a-b). With faster freezing, on the other hand, more and smaller ice crystallites are formed. This results in smaller sheets (Figure 5c-d). Even faster freezing leads to the cellular growth of the ice template and further interconnection of the cryoaerogel sheets (Figure 5e-f). Finally, at the lowest used cooling temperature, there is additional dendrite growth, which leads to further interconnected sheets within the cryoaerogel network (Figure 5g-h).

These effects can not only be seen in cryoaerogel coatings but also in similarly frozen self-supported (that is substrate-

https://doi.org/10.1021/acs.langmuir.0c03619
Langmuir 2021, 37, 5109−5117

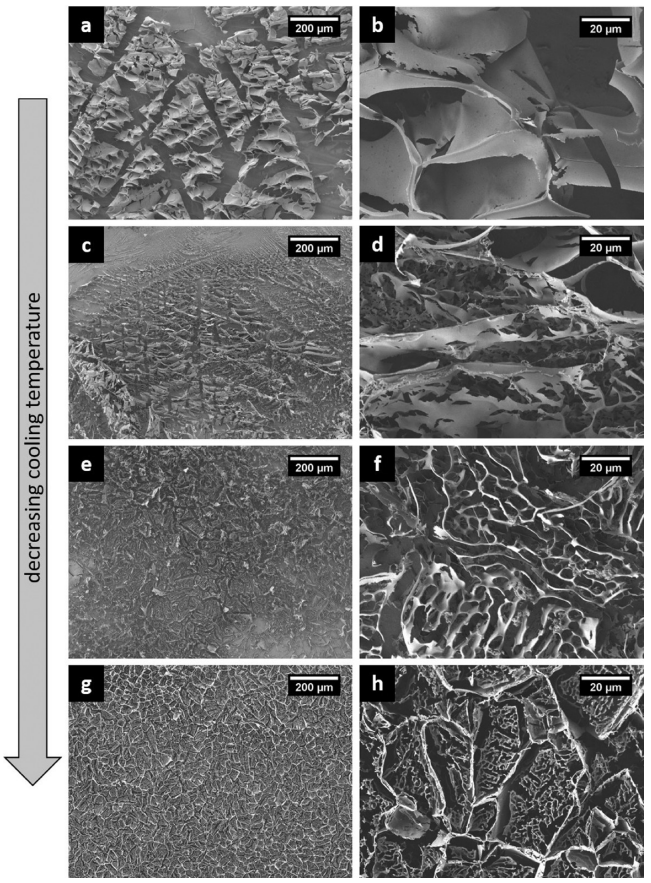

Figure 5. SEM images of platinum cryoaerogel coatings freeze-dried after flash-freezing in isopentane at different temperatures: (a-b) 263 K, (c-d) 223 K, (e-f) 173 K, and (g-h) 113 K.

free), monolithic networks. Figure 6 comparably displays the SEM images of self-supporting cryoaerogels prepared under the same conditions and with the same freezing temperatures as the cryoaerogel coatings shown in Figure 5. Like for those samples, here, we observed smaller sheet sizes in the network with lower freezing temperatures too.

It is further notable that the average aspect ratio of the sheets forming the gels increases with lower temperatures. The average sizes that were measured from the SEM images with the software *ImageJ* are presented in Table 2.

In addition to smaller sheet sizes, from the SEM images, an increasing stability of the gel material is suspected with lower cooling temperatures: while slow freezing at 263 K causes entirely collapsed networks after freeze-drying (Figure 6a-b), faster freezing with 223 K (Figure 6c-d) and 173 K (Figure 6e-f) results in less-collapsed monoliths. Freezing at 113 K (Figure 6g-h) completely preserves the cryoaerogel network. Comparable to Figure 5, this gain in stability may be caused by progressive interconnection within the gel network, when frozen faster. It needs to be mentioned that the general stability of noble-metal aerogels is quite poor, which is attributed to the filigree, open porous network. This also prevents the possibility to perform conventional tests for mechanical stability, which lead to the destruction of the material immediately. Nevertheless, even if the stability is still not sufficient, with the special view of the SEM images shown in Figure 6, the poor stability of metal cryoaerogels is suspected to be improved with higher freezing rates because the preservation of the monolithic network is improved.

2.3. Improvements by Longer Freezing Periods. In addition to the freezing medium and temperature, we also examined the effect of different freezing times. For this, again, a concentrated platinum nanoparticle solution was applied and spread on substrates using the doctor blade method. Afterward, comparable to the standard procedure, the samples were flash-frozen with liquid nitrogen, but this time, we stored the samples in the frozen state (at 77 K) for different periods of time before freeze-drying. The freezing time ranged from 10 min (which is the standard procedure) up to 72 h. The morphology of cryoaerogel coatings thus obtained were investigated by SEM. Figure 7 compares the resulting images for a selection of different freezing periods. Further images can be seen in Figure S9.

As already mentioned, when dipping a substrate coated with the nanoparticle solution in liquid nitrogen, because of its low boiling point, nitrogen evaporates and forms a bubble wrap around the sample. The resulting low heat conductivity in combination with the fact that the bottom of the substrate comes into contact with the freezing medium first leads to a temperature gradient from the bottom to the top of the sample. In this way, the lamellar freezing of ice crystals perpendicular to the substrate surface takes place.[38] Because the nanoparticles are pushed into the crystal boundaries during this step, the final cryoaerogel consists of sheetlike-shaped networks standing upright on the substrate. With a prolonged freezing duration, over the first hours, a continuous improvement in the network structure was observed regarding covering and homogeneity. Maximum improvement was achieved after 24 h in the frozen state. Longer freezing periods caused no further improvement but showed the same (highest) quality. In the case of freeze-casting, it has already been shown that short freezing gives particles insufficient time to rearrange and causes poor particle packing.[39,40] Therefore, we suppose that prolonged time within the ice template leads to the progressive rearrangement and gelation of the particles. Also, the attachment to the substrate surface is improved. In case of shorter durations (less than 24 h), these connections are partially incomplete or not strong enough; hence, no sufficiently stable network is left after ice template removal. For this reason, the resulting aerogel sheets partially collapse and/or detach from the substrate during or after lyophilization.

To quantify the improvement by longer freezing periods, we determined the remaining platinum amount within the coating via inductively coupled plasma optical emission spectroscopy (ICP-OES) after freezing for different times and subsequent freeze-drying. The results are shown in Figure 8.

For all the samples, the same amount of platinum (~0.35 mg) was used during preparation. However, we observed that the proportion of the platinum aerogel finally remaining on the substrate differed for different times of storage in the frozen state beforehand. In detail, direct lyophilization led to the least amount of aerogel, whereas the amount was increasing with longer freezing periods. In line with the results from SEM, the maximum was found after about 24 h. From this point, nearly all the initially applied platinum (97−99%) stayed on the substrate and was detected via ICP-OES. Longer periods approximately maintained this quality but led to no further improvement.

These results further indicate a relatively poor stability for cryoaerogels from the standard procedure. Without sufficient

https://doi.org/10.1021/acs.langmuir.0c03619
Langmuir 2021, 37, 5109−5117

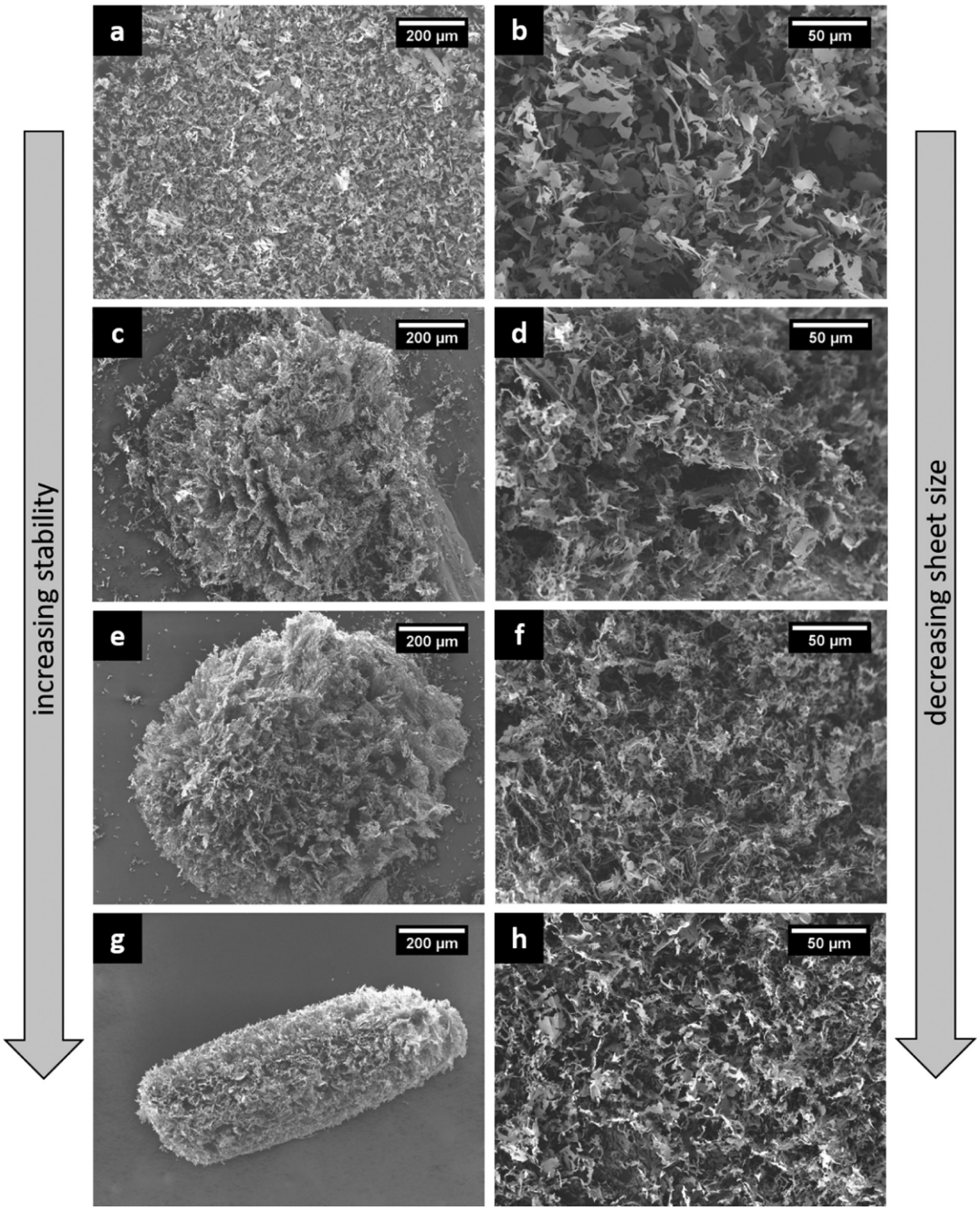

Figure 6. SEM images of substrate-free, self-supporting platinum cryoaerogels freeze-dried after flash-freezing in isopentane at different temperatures: (a-b) 263 K, (c-d) 223 K, (e-f) 173 K, and (g-h) 113 K.

Table 2. Average Sheet Sizes of Substrate-Free, Self-Supporting Cryoaerogels Freeze-Dried after Flash-Freezing in Isopentane at Different Temperatures

temperature	263 K	223 K	173 K	113 K
width [μm]	14.6 ± 2.0	8.7 ± 0.9	5.4 ± 0.7	1.9 ± 0.6
length [μm]	33.1 ± 4.9	29.1 ± 1.4	20.6 ± 1.7	18.3 ± 3.0

time before freeze-drying, the connections within the aerogel network are imperfect; hence, an early freeze-drying leads to a partial collapse and detachment from the substrate (e.g., because of air circulation). Longer freezing periods lead to progressive linkage between the particles, and by that, the cryoaerogel stability is optimized after about 24 h.

It is worth mentioning that the general stability of noble-metal aerogels is quite poor, which is attributed to the filigree, open porous network. According to that, conventional tests for mechanical stability lead to the destruction of the material immediately. Nevertheless, with regard to the potential applications, we tested the stability of platinum cryoaerogel coatings in a wet chemical environment and found similar improvements of stability by longer freezing periods (see Figure S13).

Over and above that, as long as samples are kept in the frozen state (below 273 K), the aforementioned improvement of the coating quality is independent of the storage temperature after flash-freezing, and it was also evident when

https://doi.org/10.1021/acs.langmuir.0c03619
Langmuir 2021, 37, 5109−5117

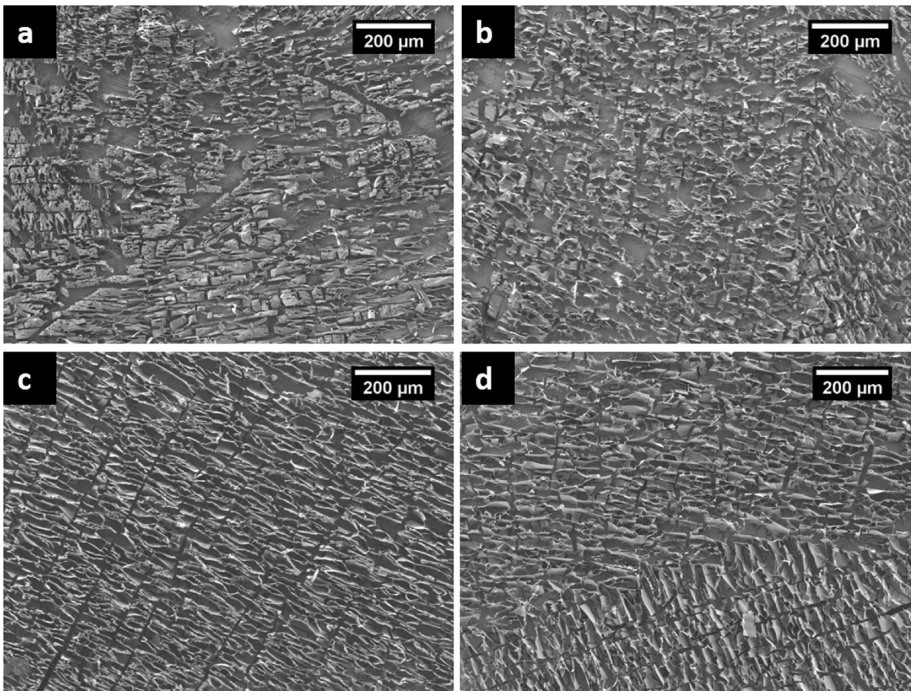

Figure 7. SEM images of platinum cryoaerogel coatings frozen with liquid nitrogen and freeze-dried after different times in the frozen state: (a) 10 min, (b) 3 h, (c) 24 h, and (d) 72 h.

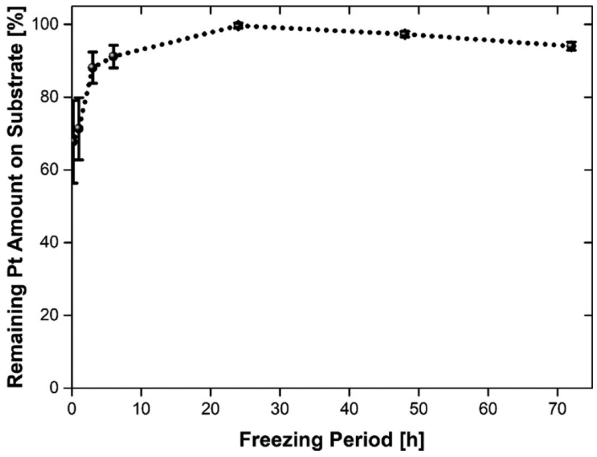

Figure 8. Platinum amounts of cryoaerogel coatings frozen and kept in liquid nitrogen for different times before freeze-drying. Determined with ICP-OES and related to the initially applied amount.

the samples were stored at other temperatures (see the results for storing at 253 K in Figures S11−S13).

3. CONCLUSIONS

We investigated the impact of different freezing media, temperatures, and freezing periods on the resulting morphology during the preparation of cryoaerogel materials. In comparison to the known standard procedure,[25] we showed that faster freezing causes very different network structures with improved stability in cryoaerogels. The obtained morphology resembles the structure of the voids between the built ice crystals. This, however, changes drastically with higher freezing rates, which are increased by lower freezing temperatures on the one hand and by cooling media with higher heat conductivities on the other hand (in that case, even at temperatures which are way above those of the standard procedure). Apart from this, we also showed that prolonged freezing (up to 24 h) of the colloid before freeze-drying increases the cryoaerogel quality.

In summary, we can create a variety of different morphologies from cryoaerogels and can further tune the network structure for targeted designs by simply adjusting the freezing period, medium, and temperature. Because of the additive-free preparation and the versatile structures, the accessible surface area of the metal aerogel coatings can be specifically adjusted in future studies. Already, the large diversity of network structures accessible combined with greatly enhanced stability shows that the cryoaerogelation of presynthesized aqueous colloidal nanoparticle suspensions is a much more versatile and promising approach for the fabrication of highly porous coatings and monoliths than previously suspected, especially when the freezing conditions are adopted properly.

4. EXPERIMENTAL SECTION/METHODS

The solutions of platinum nanoparticles were synthesized following the previously reported method.[25] We used 36.2 mL of a 0.2 wt % dihydrogen hexachloroplatinate(IV) hexahydrate solution (Alfa Aesar) and filled it with distilled water (18 MΩ cm) to a total volume of 500 mL. Under continuous stirring, this solution was boiled for 1 min at 100 °C, before 11.6 mL of a 1 wt % trisodium citrate solution was added. Thirty seconds later, 5.5 mL of 0.076 wt % ice-cold sodium borohydride solution was injected, whereupon the color of the solution turned from yellow to dark brown. The reaction is completed within a minute, and the resulting colloid can be stored under ambient conditions.

4.1. Concentration of Nanoparticle Solutions. The volume of nanoparticle solutions was reduced from 500 to 50 mL using a solvent-resistant ultrafiltration cell (Merck Millipore), a 10 kDa polyethersulfon membrane (Sartorius Stedim), and a pressure of 5 bar. Afterward, the remaining solutions were filled into the centrifuge tubes with an inbuilt filter (Amicon Ultra-15, 10 k Da, Merck Millipore). At 4000 rcf for 5 to 8 min, the solutions were reduced

https://doi.org/10.1021/acs.langmuir.0c03619
Langmuir 2021, 37, 5109−5117

stepwise to a volume of 0.25 mL. Finally, the solutions were washed three times. For this, the solutions were mixed with 5 mL of distilled water and reduced to 0.25 mL again using a centrifuge filter.

4.2. Preparation of Substrates. For our substrates, we cut ITO-coated glass to pieces of dimensions 1.5 × 1.0 cm and modified their surface with (3-aminopropyl)triethoxysilane (APTMS). For this, we activated the surface of the glass substrates in the first step by immersing them in a mixture of 40 mL of distilled water, 8 mL of hydrogen peroxide (30%, Sigma Aldrich), and 8 mL of ammonium hydroxide solution (25 wt %, Sigma Aldrich). Under continuous stirring, the solution was heated to 50 °C for 30 min. Afterward, the activated glass substrates were rinsed with distilled water and isopropanol (Merck) and dried with compressed air. In a second step, the activated glass substrates were modified with APTMS. They were immersed in a solution of 0.15 mL of APTMS (Acros) in 60 mL of toluene (Sigma Aldrich) and heated to 70 °C for 2 h under continuous stirring. Afterward, the modified substrates were rinsed with toluene and dried with compressed air.

4.3. Cryoaerogelation. To prepare the cryoaerogel coatings, defined square-shaped areas (0.5 × 0.5 cm) were masked on the modified glass substrates using a scotch tape. Afterward, a total amount of 1 μL of the concentrated nanoparticle solution was applied to the substrate and distributed uniformly on the area to be coated. The samples were then flash-frozen by dipping in the respective freezing medium (that was cooled to the respective temperature with liquid nitrogen) for 10 min to 72 h. Subsequently, the samples were freeze-dried in a lyophilizer (Christ Alpha 1−2 LD+) at 0.04 mbar for 18 h. To prepare self-supporting, monolithic cryoaerogels, a total amount of 50 μL of the concentrated nanoparticle solution was flash-frozen by injecting it directly into a vial with the cooling medium for 10 min before freeze-drying. All the received cryoaerogels were stored under ambient conditions.

4.4. SEM. For SEM, a JEOL JFM 6700F electron microscope was operated at 2 kV. Self-supported, monolithic cryoaerogels were placed onto adhesive carbon polymer pads. Substrates with cryoaerogel coatings were placed onto the adhesive carbon polymer pads and glued with silver lacquer.

4.5. TEM. TEM was performed with a FEI Tecnai G2 F20 electron microscope operated at 200 kV. Samples were prepared by carefully touching cryoaerogels with a TEM grid (copper mesh covered with a carbon film, Quantifoil).

4.6. ICP-OES. For analyzing the platinum amount, each sample was dissolved in 2 mL of aqua regia, which was prepared by mixing hydrochloric acid (37%, Fluka) and nitric acid (65%, Sigma Aldrich) in a ratio of 3:1. After 1 d, the solutions were filled with nitric acid (4%) to a volume of 25 mL and measured with a 5110 ICP-OES from Agilent Technologies. For calibration, solutions with defined concentrations (0, 0.5, 1.25, 2.5, 5, and 10 mg L^{-1}) were produced by the use of the platinum standard solution (Fluka). Each sample was measured at three different wavelengths (203.646, 214.424, and 217.468 nm), and each measurement was reproduced with three samples.

■ ASSOCIATED CONTENT

Supporting Information

The Supporting Information is available free of charge at https://pubs.acs.org/doi/10.1021/acs.langmuir.0c03619.

Characterization of platinum nanoparticles; photographs and (HR-)TEM images of the investigated samples; further information regarding longer freezing periods; and specific surface area measurements (PDF)

■ AUTHOR INFORMATION

Corresponding Author

Dirk Dorfs − *Institute of Physical Chemistry and Electrochemistry, Leibniz Universität Hannover, Hannover 30167, Germany; Laboratory for Nano and Quantum Engineering, Leibniz Universität Hannover, Hannover 30167, Germany; Cluster of Excellence PhoenixD (Photonics, Optics and Engineering − Innovation Across Disciplines), Hannover 30167, Germany*; Email: dirk.dorfs@pci.uni-hannover.de

Authors

Dennis Müller − *Institute of Physical Chemistry and Electrochemistry, Leibniz Universität Hannover, Hannover 30167, Germany; Laboratory for Nano and Quantum Engineering, Leibniz Universität Hannover, Hannover 30167, Germany*

Lars F. Klepzig − *Institute of Physical Chemistry and Electrochemistry, Leibniz Universität Hannover, Hannover 30167, Germany; Cluster of Excellence PhoenixD (Photonics, Optics and Engineering − Innovation Across Disciplines), Hannover 30167, Germany*

Anja Schlosser − *Institute of Physical Chemistry and Electrochemistry, Leibniz Universität Hannover, Hannover 30167, Germany; Laboratory for Nano and Quantum Engineering, Leibniz Universität Hannover, Hannover 30167, Germany*

Nadja C. Bigall − *Institute of Physical Chemistry and Electrochemistry, Leibniz Universität Hannover, Hannover 30167, Germany; Laboratory for Nano and Quantum Engineering, Leibniz Universität Hannover, Hannover 30167, Germany; Cluster of Excellence PhoenixD (Photonics, Optics and Engineering − Innovation Across Disciplines), Hannover 30167, Germany*; orcid.org/0000-0003-0171-1106

Complete contact information is available at: https://pubs.acs.org/10.1021/acs.langmuir.0c03619

Author Contributions

The manuscript was written through contributions of all authors. All authors have given approval to the final version of the manuscript.

Funding

The project has in parts been funded by the Deutsche Forschungsgemeinschaft (DFG, German Research Foundation) under Germany's Excellence Strategy within the Cluster of Excellence PhoenixD (EXC 2122, Project ID 390833453). The authors also would like to acknowledge the DFG (grant agreement BI 1708/4−1 & DO 1580/5−1), the European Research Council (European Un-ion's Horizon 2020 research and innovation program, grant agreement 714429), and the German Federal Ministry of Education and Research (BMBF) within the framework of the program Nano-MatFutur (support code 03X5525) for financial support.

Notes

The authors declare no competing financial interest.

■ ACKNOWLEDGMENTS

A. S. is thankful for the financial support from the Hannover School for Nanotechnology (HSN). D.M. is thankful for the financial support from the Graduiertenakademie of the Leibniz Universität Hannover. The authors thank Armin Feldhoff and Jürgen Caro for providing the SEM facility as well as the Institute for Inorganic Chemistry for providing the ICP-OES facility.

■ REFERENCES

(1) Zhou, C.; Shi, J.; Zhou, W.; Cheng, K.; Zhang, Q.; Kang, J.; Wang, Y. Highly Active ZnO-ZrO_2 Aerogels Integrated with H-ZSM-

5 for Aromatics Synthesis from Carbon Dioxide. *ACS Catal.* **2020**, *10*, 302−310.
(2) Shi, Q.; Zhu, W.; Zhong, H.; Zhu, C.; Tian, H.; Li, J.; Xu, M.; Su, D.; Li, X.; Liu, D.; Xu, B. Z.; Beckman, S. P.; Du, D.; Lin, Y. Highly Dispersed Platinum Atoms on the Surface of AuCu Metallic Aerogels for Enabling H_2O_2 Production. *ACS Appl. Energy Mater.* **2019**, *2*, 7722−7727.
(3) Zion, N.; Cullen, D. A.; Zelenay, P.; Elbaz, L. Heat-Treated Aerogel as a Catalyst for the Oxygen Reduction. *Angew. Chem., Int. Ed.* **2020**, *59*, 2483−2489.
(4) Oztuna, F. E. S.; Beyazay, T.; Unal, U. Facile Synthesis of Graphene Aerogel Supported Nickel/Nickel Oxide Core-Shell Nanoparticles: Efficient Electrocatalysts for Oxygen Evolution Reactions. *J. Phys. Chem. C* **2019**, *123*, 28131−28141.
(5) Fan, W.; Wang, D.; Sun, Z.; Ling, X. Y.; Liu, T. Graphene/Graphene Nanoribbon Aerogels Decorated with S-Doped MoSe2 Nanosheets as an Efficient Electrocatalyst for Hydrogen Evolution. *Inorg. Chem. Front.* **2019**, *6*, 1209−1216.
(6) Tang, S.; Ran, J.; Guo, J.; Tang, A. Preparation of Highly Stable and Effective N-Doped TiO2@SiO2 Aerogel Catalyst for Degradation of Organic Pollutants by Visible Light Catalysis. *J. Chem.* **2019**, *2019*, 1−10.
(7) Zhu, C.; Xu, J.; Song, S.; Wang, J.; Li, Y.; Liu, R.; Shen, Y. TiO2 Quantum Dots Loaded Sulfonated Graphene Aerogel for Effective Adsorption-Photocatalysis of PFOA. *Sci. Total Environ.* **2020**, *698*, No. 134275.
(8) Yang, J.; Li, Y.; Zheng, Y.; Xu, Y.; Zheng, Z.; Chen, X.; Liu, W. Versatile Aerogels for Sensors. *Small* **2019**, *15*, No. 1902826.
(9) Luo, Q.; Zheng, H.; Hu, Y.; Zhuo, H.; Chen, Z.; Peng, X.; Zhong, L. Carbon Nanotube/Chitosan-Based Elastic Carbon Aerogel for Pressure Sensing. *Ind. Eng. Chem. Res.* **2019**, *58*, 17768−17775.
(10) Shao, G.; Ovsianytskyi, O.; Bekheet, M. F.; Gurlo, A. On-chip Assembly of 3D Graphene-Based Aerogels for Chemiresistive Gas Sensing. *Chem. Commun.* **2020**, *56*, 450.
(11) Jiang, Q.; Xu, P.; Sun, M. Resorcinol−Formaldehyde Aerogel Coating for In-Tube Solid-Phase Microextraction of Estrogens. *J. Sep. Sci.* **2020**, 1323−1330.
(12) Pekala, R. W.; Farmer, J. C.; Alviso, C. T.; Tran, T. D.; Mayer, S. T.; Miller, J. M.; Dunn, B. Carbon Aerogels for Electrochemical Applications. *J. Non-Cryst. Solids* **1998**, *225*, 74−80.
(13) Budunoglu, H.; Yildirim, A.; Guler, M. O.; Bayindir, M. Highly Transparent, Flexible, and Thermally Stable Superhydrophobic ORMOSIL Aerogel Thin Films. *ACS Appl. Mater. Interfaces* **2011**, *3*, 539−545.
(14) Liu, W.; Herrmann, A.-K.; Geiger, D.; Borchardt, L.; Simon, F.; Kaskel, S.; Gaponik, N.; Eychmüller, A. High-Performance Electrocatalysis on Palladium Aerogels. *Angew. Chem., Int. Ed.* **2012**, *51*, 5743−5747.
(15) Liu, W.; Rodriguez, P.; Borchardt, L.; Foelske, A.; Yuan, J.; Herrmann, A.-K.; Geiger, D.; Zheng, Z.; Kaskel, S.; Gaponik, N.; Kötz, R.; Schmidt, T. J.; Eychmüller, A. Bimetallic Aerogels: High-Performance Electrocatalysts for the Oxygen Reduction Reaction. *Angew. Chem., Int. Ed.* **2013**, *52*, 9849−9852.
(16) Mao, J.; Wu, F.-F.; Shi, W.-H.; Liu, W.-X.; Xu, X.-L.; Cai, G.-F.; Li, Y.-W.; Cao, X.-H. Preparation of Polyaniline-coated Composite Aerogel of MnO_2 and Reduced Graphene Oxide for High-performance Zinc-ion Battery. *Chin. J. Polym. Sci.* **2020**, *38*, 514−521.
(17) Liu, W.; Herrmann, A.-K.; Bigall, N. C.; Rodriguez, P.; Wen, D.; Oezaslan, M.; Schmidt, T. J.; Gaponik, N.; Eychmüller, A. Noble Metal Aerogels - Synthesis, Characterization, and Application as Electrocatalysts. *Acc. Chem. Res.* **2015**, *48*, 154−162.
(18) Deville, S. Freeze-Casting of Porous Ceramics: A Review of Current Achievements and Issues. *Adv. Eng. Mater.* **2008**, *10*, 155−169.
(19) Deville, S. Freeze-Casting of Porous Biomaterials: Structure, Properties and Opportunities. *Materials* **2010**, *3*, 1913−1927.
(20) Gutiérrez, M. C.; Ferrer, M. L.; del Monte, F. Ice-Templated Materials: Sophisticated Structures Exhibiting Enhanced Functionalities Obtained after Unidirectional Freezing and Ice-Segregation-Induced Self-Assembly. *Chem. Mater.* **2008**, *20*, 634−648.
(21) Rogers, Z. J.; Bencherif, S. A. Cryogelation and Cryogels. *Gels* **2019**, *5*, 46.
(22) Hixon, K. R.; Lu, T.; Sell, S. A. A Comprehensive Review of Cryogels and Their Roles in Tissue Engineering Applications. *Acta Biomater.* **2017**, *62*, 29−41.
(23) Memic, A.; Colombani, T.; Eggermont, L. J.; Rezaeeyazdi, M.; Steingold, J.; Rogers, Z. J.; Navare, K. J.; Mohammed, H. S.; Bencherif, S. A. Latest Advances in Cryogel Technology for Biomedical Applications. *Adv. Therap.* **2019**, *2*, No. 1800114.
(24) Bencherif, S. A.; Braschler, T. M.; Renaud, P. Advances in the Design of Macroporous Polymer Scaffolds for Potential Applications in Dentistry. *J. Periodontal. Implant Sci.* **2013**, *43*, 251−261.
(25) Freytag, A.; Sánchez-Paradinas, S.; Naskar, S.; Wendt, N.; Colombo, M.; Pugliese, G.; Poppe, J.; Demirci, C.; Kretschmer, I.; Bahnemann, D. W.; Behrens, P.; Bigall, N. C. Versatile Aerogel Fabrication by Freezing and Subsequent Freeze-Drying of Colloidal Nanoparticle Solutions. *Angew. Chem., Int. Ed.* **2016**, *55*, 1200−1203.
(26) Freytag, A.; Colombo, M.; Bigall, N. C. Catalytic Properties of Cryogelated Noble Metal Aerogels. *Z. Phys. Chem.* **2017**, *231*, 63−75.
(27) Kodanek, T.; F reytag, A.; Schlosser, A.; Naskar, S.; Härtling, T.; Dorfs, D.; Bigall, N. C. Macroscopic Aerogels with Retained Nanoscopic Plasmonic Properties. *Z. Phys. Chem.* **2018**, *232*, 1675−1689.
(28) Schlosser, A.; Meyer, L. C.; Lübkemann, F.; Miethe, J. F.; Bigall, N. C. Nanoplatelet Cryoaerogels with Potential Application in Photoelectrochemical Sensing. *Phys. Chem. Chem. Phys.* **2019**, *21*, 9002.
(29) Cai, B.; Eychmüller, A. Promoting Electrocatalysis upon Aerogels. *Adv. Mater.* **2019**, *31*, No. 1804881.
(30) Nelson, I.; Naleway, S. E. Intrinsic and Extrinsic Control of Freeze Casting. *J. Mater. Res. Technol.* **2019**, *8*, 2372−2385.
(31) Wang, C.; Chen, X.; Wang, B.; Huang, M.; Wang, B.; Jiang, Y.; Ruoff, R. S. Freeze-Casting Produces a Graphene Oxide Aerogel with a Radial and Centrosymmetric Structure. *ACS Nano* **2018**, *12*, 5816−5825.
(32) Zhang, L.; Kiu, X.; Deb, A.; Feng, G. Ice-Templating Synthesis of Hierarchical and Anisotropic Silver-Nanowire-Fabric Aerogel and Its Application for Enhancing Thermal Energy Storage Composites. *ACS Sustainable Chem. Eng.* **2019**, *7*, 19910−19917.
(33) Lottermoser, A. Über das Ausfrieren von Hydrosolen. *Ber. Dtsch. Chem. Ges.* **1908**, *41*, 3976−3979.
(34) Makkonen, L. Solid Fraction in Dendritic Solidification of a Liquid. *Appl. Phys. Lett.* **2010**, *96*, No. 091910.
(35) Klug, D. D. Glassy Waters. *Science* **2001**, *294*, 2305−2306.
(36) Fahy, G. M.; MacFarlane, D. R.; Angell, C. A.; Meryman, H. T. Vitrification as an Approach to Cryopreservation. *Cryobiology* **1984**, *21*, 407−426.
(37) Muslumova, S.; Yetiskin, B.; Okay, O. Highly Stretchable and Rapid Self-Recoverable Cryogels Based on Butyl Rubber as Reusable Sorbent. *Gels* **2019**, *5*, 1.
(38) Deville, S.; Saiz, E.; Tomsia, A. P. Ice-Templated Porous Alumina Structures. *Acta Mater.* **2007**, *55*, 1965−1974.
(39) Naglieri, V.; Bale, H. A.; Gludovatz, B.; Tomsia, A. P.; Ritchie, R. O. On the Development of Ice-Templated Silicon Carbide Scaffolds for Nature-Inspired Structural Materials. *Acta Mater.* **2013**, *61*, 6948−6957.
(40) Farhangdoust, S.; Zamanian, A.; Yasaei, M.; Khorami, M. The Effect of Processing Parameters and Solid Concentration on the Mechanical and Microstructural Properties of Freeze-Casted Macroporous Hydroxyapatite Scaffolds. *Mater. Sci. Eng.: C* **2013**, *33*, 453−460.

https://doi.org/10.1021/acs.langmuir.0c03619
Langmuir 2021, 37, 5109−5117